

## Why is longwave cloud feedback positive?

Mark D. Zelinka<sup>1</sup> and Dennis L. Hartmann<sup>1</sup>

Received 6 January 2010; revised 29 March 2010; accepted 29 April 2010; published 25 August 2010.

[1] Longwave cloud feedback is systematically positive and nearly the same magnitude across all global climate models used in the Intergovernmental Panel on Climate Change Fourth Assessment Report (AR4). Here it is shown that this robust positive longwave cloud feedback is caused in large part by the tendency for tropical high clouds to rise in such a way as to remain at nearly the same temperature as the climate warms. Furthermore, it is shown that such a cloud response to a warming climate is consistent with well-known physics, specifically the requirement that, in equilibrium, tropospheric heating by convection can only be large in the altitude range where radiative cooling is efficient, following the fixed anvil temperature hypothesis of Hartmann and Larson (2002). Longwave cloud feedback computed assuming that high-cloud temperature follows upper tropospheric convergence-weighted temperature, which we refer to as proportionately higher anvil temperature, gives an excellent prediction of the longwave cloud feedback in the AR4 models. The ensemble-mean feedback of  $0.5 \text{ W m}^{-2} \text{ K}^{-1}$  is much larger than that calculated assuming clouds remain at fixed pressure, highlighting the large contribution from rising cloud tops to the robustly positive feedback. An important result of this study is that the convergence profile computed from clear-sky energy and mass balance warms slightly as the climate warms, in proportion to the increase in stability, which results in a longwave cloud feedback that is slightly smaller than that calculated assuming clouds remain at fixed temperature.

**Citation:** Zelinka, M. D., and D. L. Hartmann (2010), Why is longwave cloud feedback positive?, *J. Geophys. Res.*, *115*, D16117, doi:10.1029/2010JD013817.

### 1. Introduction

[2] In the present climate, clouds strongly cool the planet, reducing the net downwelling radiation at the top of the atmosphere by about  $20 \text{ W m}^{-2}$ . Comparing this number with the radiative forcing associated with a doubling of  $\text{CO}_2$ ,  $4 \text{ W m}^{-2}$ , it is clear that even tiny changes in clouds can have dramatic effects on the climate and can act as a positive or negative feedback on climate change. It is for this reason that understanding how clouds respond to a warming planet is of vital importance for accurately predicting how the climate will change.

[3] *Cess et al.* [1990], *Colman* [2003], *Soden and Held* [2006], and *Webb et al.* [2006] show that the largest uncertainty in global climate model (GCM) projections of future climate change is caused by the responses of clouds to a warming climate. Whereas other feedbacks are similar among the models, the cloud feedback varies between  $0.14$  and  $1.18 \text{ W m}^{-2} \text{ K}^{-1}$  [*Soden and Held*, 2006] and little progress has been made in reducing this spread. *Bony et al.* [2006] point out several reasons why progress has been slow in evaluating cloud feedbacks and narrowing this range. It is

difficult to use observations to evaluate cloud feedback because observable climate variations are not good analogues for climate change due to increasing greenhouse gases and because it is nearly impossible to isolate the unambiguous role of clouds in causing a change in net radiation at the top of atmosphere. Additionally, the radiative impact of clouds is large, so even subtle changes to their characteristics (height, amount, thickness, etc.) can have dramatic effects on the climate. Finally, clouds are not actually resolved in GCMs but are instead parameterized; thus a variety of plausible and self-consistent cloud responses to global warming can be produced in models.

[4] Though estimates of cloud feedback vary significantly among the Intergovernmental Panel on Climate Change Fourth Assessment Report (IPCC AR4) models [*Soden and Held*, 2006], this large spread is primarily due to the shortwave (SW) component, which can be attributed to uncertainties in simulations of the response of marine boundary layer clouds to changing conditions [*Bony and Dufresne*, 2005]. Generally speaking, the models which predict a reduction in low cloud fraction exhibit greater 21st century warming because the reduction in the area of such clouds with large negative net cloud forcing represents a strong positive cloud feedback. Conversely, the models that predict increases in low clouds have very low climate sensitivity.

[5] Whereas estimates of SW cloud feedback vary considerably such that even the sign is uncertain, estimates of

<sup>1</sup>Department of Atmospheric Sciences, University of Washington, Seattle, Washington, USA.

longwave (LW) cloud feedback are systematically positive in all AR4 models and exhibit half as much spread (B. J. Soden, personal communication, 2009). In this study we address the question of why all the AR4 models exhibit positive LW cloud feedbacks. We show that the robust positive LW cloud feedback is largely due to tropical high clouds, which remain at approximately the same temperature as the climate warms. Furthermore, we show that this cloud response should be expected from basic physics and is therefore fundamental to Earth's climate.

[6] We demonstrate this by making use of the clear-sky energy budget, which requires balance between subsidence warming and radiative cooling. Because radiative cooling by water vapor becomes very inefficient at very low temperatures, subsidence rapidly decreases with decreasing pressure in the tropical upper troposphere. This causes large convergence into the clear-sky upper troposphere, which, by mass conservation, implies large convective detrainment and abundant high cloudiness at that level. Thus the implied clear-sky upper tropospheric convergence calculated from clear-sky mass and energy balance provides a convenient marker for the level of high clouds and a diagnostic tool for understanding how that level changes as the climate warms.

[7] As described in the fixed anvil temperature (FAT) hypothesis of *Hartmann and Larson* [2002], this level should remain at approximately the same temperature as the climate warms because it is a fundamental result of radiative convective equilibrium: The troposphere can only be heated by convection where it is being sufficiently cooled by radiation, resulting in an equilibrium near neutral stability. Because the altitude range of sufficient radiative cooling by water vapor is primarily determined by temperature through the Clausius-Clapeyron relation, the temperature that marks the top of the convective cloudiness should remain approximately constant as the climate warms.

[8] In the cloud resolving model simulations of *Kuang and Hartmann* [2007], high clouds migrate upward for higher values of SST, but do so in such a way as to remain at the same temperature. The clear-sky upper tropospheric diabatic convergence calculated from the clear-sky energy balance as described above shows an identical constancy in temperature for all simulations. *Kubar et al.* [2007] showed, using MODIS observations, that the level of abundant anvil cloud tops and its seasonal and regional variability is accurately predicted by clear-sky energy budget considerations, indicating that the real atmosphere is also subject to such constraints. *Xu et al.* [2005, 2007] and *Eitzen et al.* [2009] showed, using observations from the CERES instrument on the TRMM satellite, that the distribution of tropical cloud top temperatures for clouds with tops greater than 10 km remains approximately constant as SSTs vary over the seasonal cycle, lending observational support to the FAT hypothesis. Conversely, *Chae and Sherwood* [2010] showed that cloud top temperatures observed by MISR exhibit appreciable fluctuations ( $\sim 5\text{K}$ ) that can be attributed to lapse rate changes in the upper troposphere.

[9] Here we show that, as in observations and cloud resolving models, clouds in the AR4 GCMs remain at approximately the same temperature as the climate warms, and that this feature is well diagnosed by the clear-sky energy budget explained above. This is perhaps unsurprising

given that it is a result that arises directly from tropical radiative-convective equilibrium that GCMs must approximately maintain, regardless of the details of their individual convective and cloud parameterizations. What is less appreciated is that this important result gives rise to a robustly positive LW cloud feedback that can be explained from the fundamental principles of saturation vapor pressure, radiative transfer, and energy balance.

[10] In the first part of the paper, we assess the degree to which the model cloud fields are in agreement with the basic physics described above, both in the mean sense and as the climate warms. In the second part, we decompose the LW cloud feedback into its individual components to show that the systematic tendency for GCMs to maintain nearly constant tropical high-cloud temperature causes a robust positive LW cloud feedback.

## 2. Data

[11] We make use of monthly mean model diagnostics from the IPCC SRES A2 scenario simulations that are archived at the Program for Climate Model Diagnosis and Intercomparison (PCMDI). We calculate decadal-mean quantities between the years 2000 and 2100, but maintain the monthly mean resolution such that the radiative calculations are more accurate. LW and SW radiative fluxes at both the surface and top of atmosphere and for both clear and all-sky conditions are used, as well as profiles of temperature ( $T$ ), specific humidity ( $q$ ), and cloud amount. We interpolate all quantities onto the same latitude, longitude, and pressure grid as that of the radiative kernels of *Soden et al.* [2008].

[12] Unfortunately, cloud optical thickness or effective cloud top temperature as would be seen from satellites are not standard model diagnostics available in the PCMDI archive. Only a small number of modeling centers have participated in the Cloud Feedback Model Intercomparison Project (CFMIP), in which ISCCP simulators are run in the models to better compare with observations. We instead make use of the basic cloud field that all modeling centers are required to output, the height-resolved cloud fraction within each pressure bin. This gross cloud field may include cloud types that are not relevant to this study (e.g., subvisible tropopause cirrus) as well as clouds that are not directly influencing the *OLR* (e.g., interior of clouds rather than cloud tops). Nevertheless, the cloud changes in this study are quite coherent in the sense that the entire cloud profile tends to shift to higher altitudes as the climate warms rather than exhibiting a fundamental change in shape. Thus, we can make reasonable assumptions about the cloud top properties without actually making use of optical depth or cloud top information.

## 3. Methodology

[13] Before assessing how realistically high clouds are being simulated in the models, we first demonstrate a method of calculating the altitudes of convective detrainment and implied abundant cloudiness using the tropospheric mass and energy budget equations. We adopt the same one-dimensional diagnostic model employed by

Minschwaner and Dessler [2004], Folkins and Martin [2005], Kuang and Hartmann [2007], and Kubar *et al.* [2007]. The tropical atmosphere is divided into a convective domain and a clear-sky domain. The cloudy domain is assumed to cover a small fraction of the Tropics (as active convection does in reality), with the majority of the Tropics being convection free. We shall refer interchangeably to the convective (nonconvective) region as the cloudy (clear-sky) region, though these are used very loosely simply to distinguish between regions that are undergoing active deep convection and those that are not. Most likely there are boundary layer clouds and/or nonconvective high clouds in the clear-sky region.

[14] One can write the dry static energy ( $s = c_p T + gz$ ) budget of the troposphere as

$$\frac{\partial s}{\partial t} = -\nabla \cdot (s\mathbf{U}) - c_p Q_R + SH + LP, \quad (1)$$

where  $c_p$  is the specific heat of air at constant pressure,  $Q_R$  is the net (LW plus SW) radiative cooling of the atmosphere,  $SH$  is the surface sensible heat flux,  $L$  is the latent heat of vaporization, and  $P$  is the precipitation rate. We calculate  $Q_R$  using each model's  $T$  and  $q$  profiles as input to the Fu-Liou radiation model, which uses the delta-four-stream approximation and correlated  $k$ -distribution scheme [Fu and Liou, 1992]. Although we use  $T$  and  $q$  profiles from regions that are both cloudy and clear, the radiative transfer calculation is performed assuming no clouds. Because the presence of clouds alters cooling rates substantially [e.g., Ackerman *et al.*, 1988; Stephens *et al.*, 1994; Bergman and Hendon, 1998; Sohn, 1999; L'Ecuyer and McGarragh, 2010], it is preferable to take into account clouds in the nonconvective regions. It would be very difficult to do this, however, because there is inadequate cloud property information provided by the modeling centers (e.g., particle size, phase, ice water content). Thus, we do not attempt to account for the effect of clouds on  $Q_R$  and acknowledge a small degree of uncertainty in the cooling profiles.

[15] Considering only regions of the free troposphere that are not actively convecting (such that we can ignore  $SH$  and  $LP$ ), and assuming no tendency or horizontal transport gives

$$\omega = \frac{Q_R}{\sigma} \quad (2)$$

where  $\sigma$  is the static stability, having various equivalent forms, including

$$\sigma = -\frac{T}{\theta} \frac{\partial \theta}{\partial p} = \frac{\kappa T}{p} - \frac{\partial T}{\partial p} = \frac{\Gamma_d - \Gamma}{\rho g}, \quad (3)$$

where  $\theta$  is potential temperature,  $\kappa = R_d/c_p$ ,  $\Gamma_d$  is the dry adiabatic lapse rate, and  $\Gamma$  is the lapse rate. We will refer to  $\omega$  as the diabatic vertical velocity (positive downward). From equation (2), we see that  $Q_R$  is balanced by diabatic subsidence in the clear-sky regions of the tropical free troposphere. The stronger the radiative cooling or the weaker the static stability, the larger the diabatic subsidence that is required to maintain energy balance. The energy equivalent of this diabatic subsidence is provided by convective heating.

[16] Assuming mass continuity, the diabatic convergence profile in the clear-sky region is calculated by

$$-\nabla_H \cdot \mathbf{U} = \frac{\partial \omega}{\partial p}, \quad (4)$$

where  $-\nabla_H \cdot \mathbf{U}$  is the horizontal diabatic convergence, hereafter referred to as *conv*. Assuming a closed mass budget between convective and nonconvective regions, convergence into the nonconvective region is balanced at the same altitudes by divergence out of the convective region, and vice versa. Note that using this system of equations we can calculate the implied convective detrainment simply from mass and energy conservation without invoking any complex moist physics or assumptions about parcel entrainment. This is a simple and elegant method for diagnosing the level of detrainment and abundant high clouds in the model and for understanding the changes in high clouds that accompany climate change.

[17] Rather than computing  $Q_R$  profiles corresponding to 24 solar zenith angles for each latitude and longitude in every month in every model, we instead linearize the computation about a mean  $Q_R$  profile to increase efficiency. A mean  $Q_R$  profile is calculated at each latitude and month using the ensemble-mean, monthly mean, zonal-mean  $T$  and  $q$  profiles averaged over the first decade of the 21st century. Then, perturbed  $Q_R$  profiles are calculated at each latitude and month for small perturbations at each pressure level of the  $T$  and  $q$  fields. The perturbations are as given by Soden *et al.* [2008], namely, a  $T$  increase of 1 K and an increase of  $q$  equal to that which is necessary to maintain constant RH in the presence of a 1 K increase in  $T$ . The actual  $T$  and  $q$  fields at any location and time within any model are then multiplied by the appropriate  $T$ - and  $q$ -perturbed  $Q_R$  profiles and summed to calculate the actual  $Q_R$  profile for that location. A sample of randomly selected  $Q_R$  profiles calculated using this procedure are nearly identical to those calculated by running the Fu-Liou code.

## 4. Results

[18] The tropical-mean ensemble-mean  $q$ ,  $T$ ,  $Q_R$ ,  $\sigma$ , and diabatic  $\omega$  profiles are plotted as functions of pressure in Figure 1 for averages over three decades, 2000–2010, 2060–2070, and 2090–2100. Here, ensemble mean refers to the average over the 15 models that run the A2 scenario. Note that  $q$  is plotted on a logarithmic scale.

[19] Tropospheric temperatures are nearly moist adiabatic [Xu and Emanuel, 1989], decreasing modestly with decreasing pressure in the lower troposphere, then decreasing more dramatically with decreasing pressure in the mid and upper troposphere (not shown). Water vapor concentrations are fundamentally limited by temperature through the Clausius-Clapeyron relation, thus  $q$  decreases exponentially with decreasing pressure throughout the troposphere (Figure 1a). The radiative cooling rate,  $Q_R$ , is approximately constant with pressure throughout most of the troposphere at about  $1.5 \text{ K d}^{-1}$  (Figure 1b). At the very low temperatures characteristic of the upper troposphere, water vapor concentrations become so low that  $Q_R$  dramatically falls off until reaching a level of zero radiative heating. Consistent with the sharp drop in water vapor

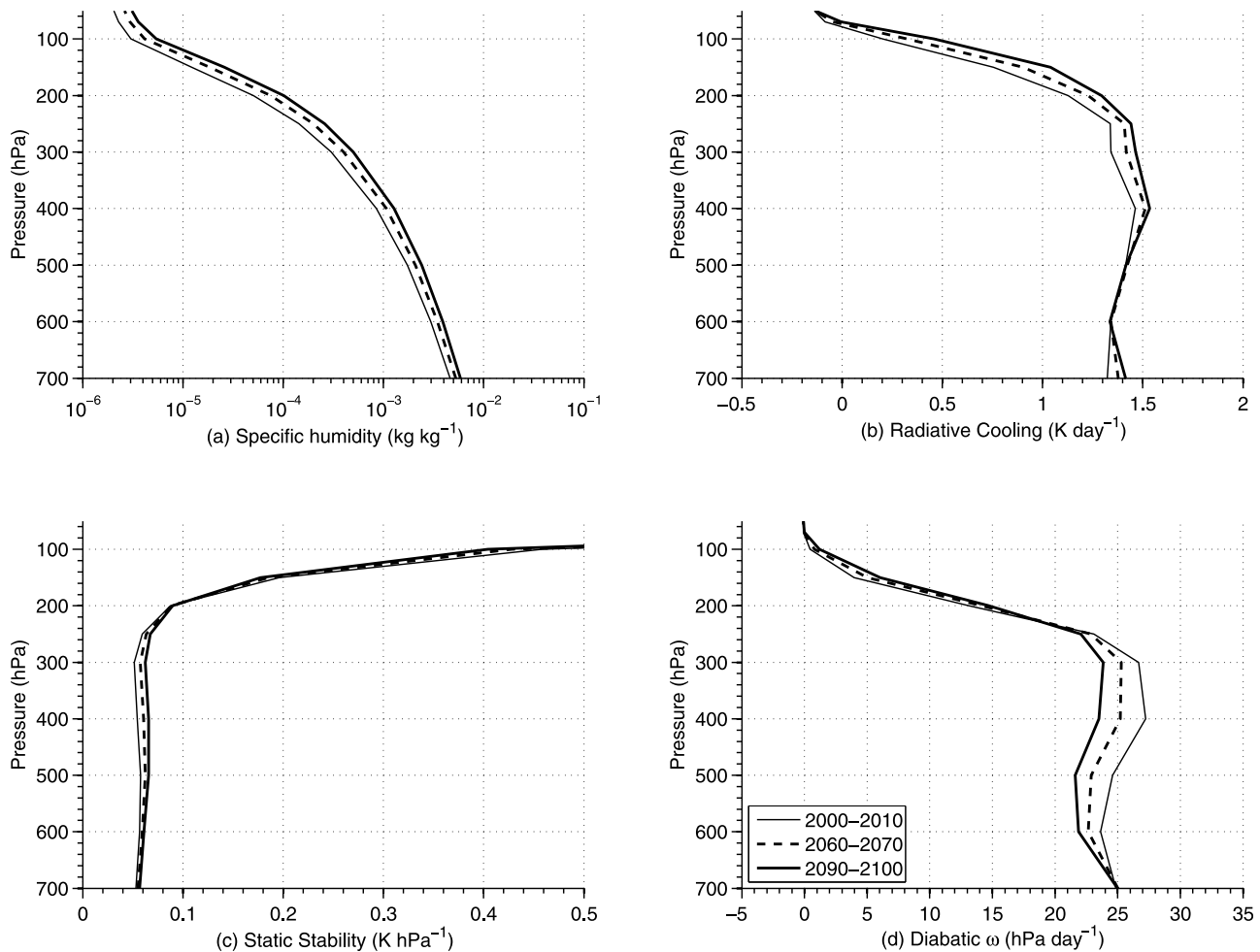


**Figure 1.** (a) Tropical-mean ensemble-mean specific humidity, (b) radiative cooling, (c) static stability, and (d) diabatic subsidence for 2000–2010 (thin solid), 2060–2070 (dashed), and 2090–2100 (thick solid). Ensemble-mean refers to the average over the 15 models that run the A2 scenario. Note that the specific humidity is plotted on a logarithmic scale.

radiative cooling, *Hartmann et al.* [2001] show that the radiative relaxation time sharply increases near 200 hPa, implying a dramatic reduction in the ability of water vapor to radiate away any temperature perturbations. Above this level, radiative processes provide net warming to the atmosphere. It is important to note that  $Q_R$  falls off to zero well below the cold-point tropopause.

[20] Static stability is small and nearly constant throughout most of the well-mixed troposphere as the  $T$  profile closely follows the moist adiabat (Figure 1c). At pressures less than about 200 hPa, the  $T$  profile becomes increasingly more stable than the moist adiabat as radiative cooling by water vapor becomes increasingly less efficient and radiative convective equilibrium is no longer the dominant balance. Additionally, the inverse pressure dependence of  $\sigma$  (equation (3)) becomes especially pronounced at these low pressures. Diabatic  $\omega$ , which is directly proportional to  $Q_R$  and inversely proportional to  $\sigma$ , very closely mimics the  $Q_R$  profile: it is nearly constant with pressure at about 25 hPa d<sup>-1</sup> throughout the troposphere, then falls off rapidly to zero in the region where  $Q_R$  falls off rapidly and  $\sigma$  increases rapidly (Figure 1d).

[21] Because the diabatic  $\omega$  is nearly constant with pressure above and below the range of altitudes where it falls off rapidly with decreasing pressure,  $conv$  (vertical derivative of  $\omega$ ) exhibits a clear peak in the upper troposphere around about 200 hPa (Figure 2). It is in this region of large upper tropospheric  $conv$  that net convective detrainment and its associated cloudiness should be maximum. Indeed, the ensemble-mean cloud amounts also exhibit a peak at the same altitude as the  $conv$  peak (Figure 2). We interpret this peak in the cloud field as due to the abundance of high clouds detrained from deep convection near the top of the region of efficient radiative cooling. The same correspondence between  $conv$  and cloud fraction is verified in MODIS observations [*Kubar et al.*, 2007] and in a cloud resolving model [*Kuang and Hartmann*, 2007].

[22] In Figure 3 we plot the change in these quantities between the beginning and end of the 21st century. Overlain in dashed and thin solid lines are the average profiles for 2000–2010 and 2090–2100, respectively. Water vapor mixing ratios increase at all levels in step with the warming climate so as to retain nearly constant relative humidity through the 21st century (Figure 3a). The amplification of

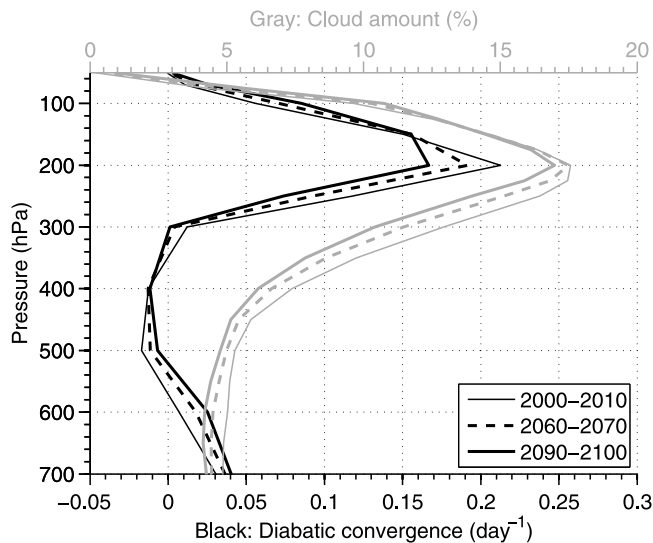


**Figure 2.** Tropical-mean ensemble-mean clear-sky diabatic convergence (black) and cloud amount (gray) for 2000–2010 (thin solid), 2060–2070 (dashed), and 2090–2100 (thick solid). Ensemble-mean refers to the average over the 15 models that run the A2 scenario.

warming aloft where water vapor concentrations are very low results in large fractional increases of  $q$  and thus very large increases in  $Q_R$  between 200 hPa and the tropopause, peaking at 150 hPa (Figure 3c). Thus, the level at which  $Q_R$  falls off rapidly shifts upward as the climate warms, as expected from the FAT hypothesis.

[23] Whereas  $Q_R$  increases everywhere throughout the middle and upper troposphere, the change in  $\sigma$  is positive at pressures greater than 200 hPa and negative at pressures less than 200 hPa (Figure 3d). Convection keeps the  $T$  profile close to the moist adiabat at pressures greater than 200 hPa; thus, the warming profile is accompanied by an increase in  $\sigma$ . The warming of the upper troposphere, which maximizes at about 200 hPa, combined with the  $\text{CO}_2$ -induced cooling of the stratosphere cause stability to decrease at pressures less than 200 hPa.

[24] At pressures greater than about 250 hPa, the fractional increase in  $\sigma$  exceeds that of  $Q_R$  (not shown), so the diabatic  $\omega$  is reduced (Figure 3e). This reduction in clear-sky  $\omega$  is consistent with several other studies that have pointed out the robust slowdown of the tropical circulation in a warmer climate [Knutson and Manabe, 1995; Held and Soden, 2006; Vecchi and Soden, 2007; Gastineau et al., 2009]. Because the fractional increase in  $\sigma$  is larger than that of  $Q_R$  at these altitudes, less  $\omega$  is required in the clear-sky atmosphere to balance the enhanced  $Q_R$ . In other words, a given descent rate achieves greater warming in the presence of enhanced  $\sigma$ .

[25] At pressures less than 200 hPa, the reduction in  $\sigma$  and increase in  $Q_R$  result in an enhancement in the diabatic  $\omega$ , or an upward shift in the  $\omega$  profile. The combination of enhanced  $\omega$  above due to enhanced  $Q_R$  and diminished  $\omega$  below due to increased  $\sigma$  reduces the vertical gradient of diabatic  $\omega$  in the warmer climate, and thus causes a reduction in the upper tropospheric  $\text{conv}$  (Figure 3f). In the end, the  $\text{conv}$  profile shifts upward along with the  $Q_R$  profile and

becomes smaller in magnitude, most dramatically at its peak, due to the competing changes in the  $Q_R$  and  $\sigma$  profiles.

[26] In summary, the warming climate is associated with two main changes to  $\text{conv}$  and implied convective detrainment. First, the location of peak  $\text{conv}$  shifts toward lower pressure. The upward shift of peak  $\text{conv}$  is consistent with upward shift in  $Q_R$  because the temperature is sufficiently “high” that there is appreciable  $Q_R$  from water vapor. As will be shown below, the upward shift is nearly isothermal, but the peak  $\text{conv}$  level warms slightly due to the significantly increased  $\sigma$ . Secondly, the upper tropospheric  $\text{conv}$  systematically decreases at all but the lowest pressures in association with the decrease in the tropical overturning circulation. Because the  $\omega$  falls off to zero less dramatically with decreasing pressure in the warmer climate as explained above, the implied upper tropospheric  $\text{conv}$  also decreases. Clearly, both the reduction in total  $\text{conv}$  and the shift toward higher altitude of peak  $\text{conv}$  are mimicked in the cloud fractions. Such a cloud response is also present in cloud resolving model simulations of *Tompkins and Craig* [1999], who noted higher but slightly warmer cloud tops as well as decreased high-cloud fractional coverage for runs at higher temperature.

[27] The quantities plotted in Figure 1 are plotted again in Figure 4, but now as a function of  $T$ . The three water vapor mixing ratio curves now lie on top of one another throughout most of the troposphere, indicating an essentially unchanged relative humidity as the climate warms (Figure 4a). Associated with this nearly unchanged relative humidity is a nearly unchanged  $Q_R$  profile, when plotted in  $T$  coordinates (Figure 4b). This clearly indicates the strong and fundamental dependence of  $Q_R$  on  $T$  through its exponential limit on the water vapor concentrations. Static stability, on the other hand, is a function of pressure and the vertical gradient of  $T$  rather than its absolute value. Thus, as the climate warms and the  $T$  profile remains locked to the moist adiabat, the  $\sigma$  at a given  $T$  increases (Figure 4c). Furthermore,  $\sigma$  is inversely dependent on pressure (equation (3)), so at a fixed temperature it increases dramatically simply because the isotherms move toward lower pressure in the warming climate.

[28] The shift toward higher  $\sigma$  at all temperatures results in a systematic decrease in diabatic  $\omega$  at all temperatures as the climate warms (Figure 4d). Although the level of peak  $\text{conv}$  shifts upward in space, it does not do so in such a way as to remain at fixed temperature. Rather, the level gets slightly warmer due to the strong increase in  $\sigma$  generated by the models (Figure 5). Similarly, the level of abundant high clouds shifts toward slightly warmer temperatures rather than staying fixed in  $T$  as would be expected from FAT (Figure 5). Modeled  $\text{conv}$  and clouds do not shift isothermally because of the strong increase in  $\sigma$  relative to  $Q_R$  that is not explicitly accounted for in the FAT mechanism. The importance of static stability changes for preventing observed cloud top temperatures from remaining constant was also emphasized by *Chae and Sherwood* [2010]. It is important to note that the clouds warm only slightly, and certainly much less than the upper troposphere. This near-constancy of cloud temperature is largely the cause of the positive LW cloud feedback, as will be shown in section 5.

[29] *Trenberth and Fasullo* [2009, Figure 3] assert that the main warming in AR4 models comes from the increase in

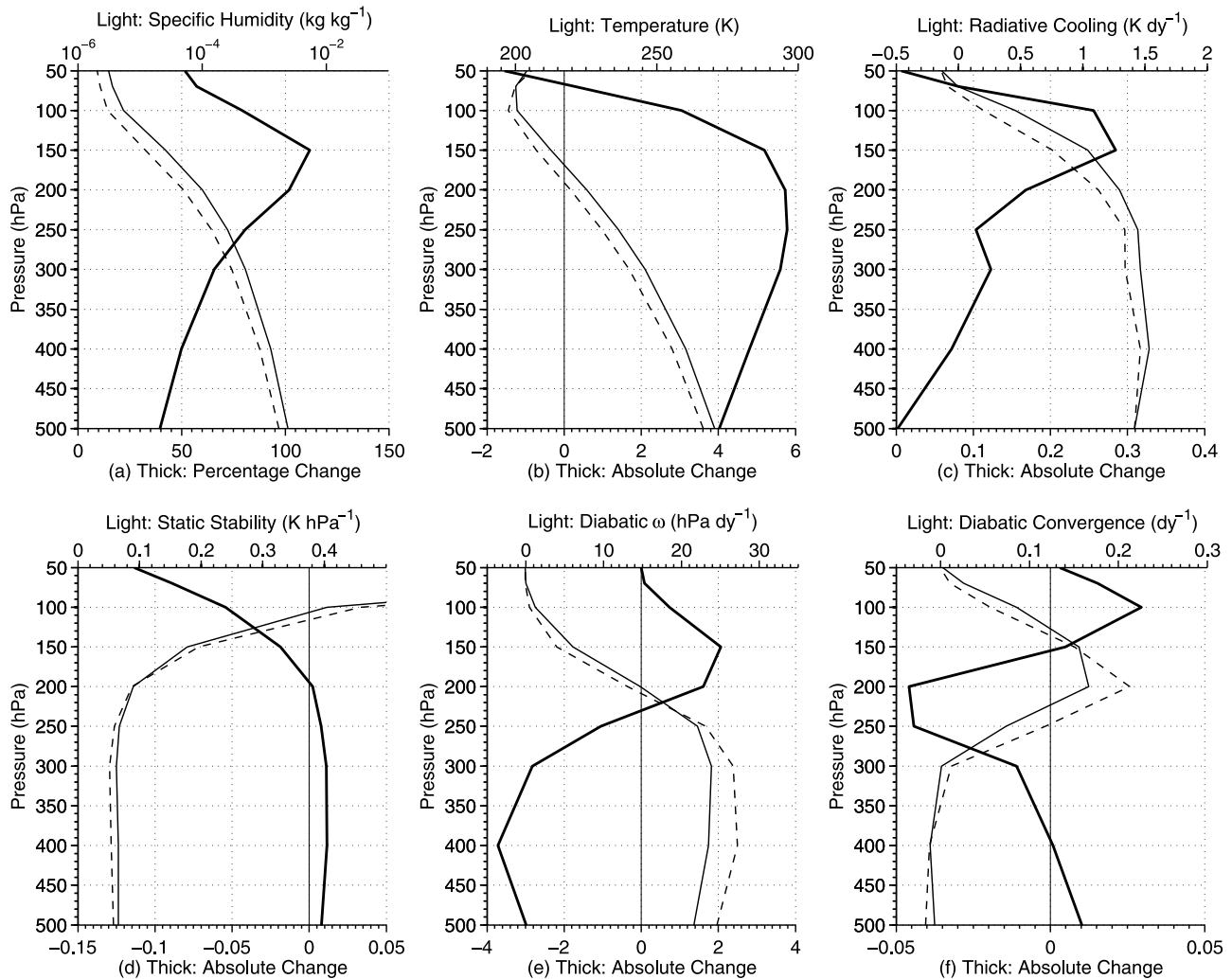


**Figure 3.** (a) Tropical-mean ensemble-mean change in specific humidity, (b) temperature, (c) radiative cooling, (d) static stability, (e) diabatic subsidence, and (f) clear-sky diabatic convergence calculated as a difference between the 2000–2010 mean and the 2090–2100 mean. Overlaid in each plot are the 2000–2010 mean (dashed line) and 2090–2100 mean (light solid line). Ensemble-mean refers to the average over the 15 models that run the A2 scenario. Note that the mean specific humidity is plotted on a logarithmic scale and its change is expressed as a percentage.

absorbed solar radiation due to decreases in tropical cloud cover. In the Tropics, the cloud fraction reduction is most evident in high clouds. Here we offer an explanation for the decrease in cloud cover, namely, the decrease in upper tropospheric *conv* that accompanies warming. As described above, the combination of enhanced  $\omega$  at pressures less than 250 hPa due to enhanced  $Q_R$  and diminished  $\omega$  at pressures greater than 250 hPa due to increased  $\sigma$  reduces the vertical gradient of diabatic  $\omega$  in the warmer climate, and thus causes a reduction in upper tropospheric *conv* (Figure 3f). These changes to  $Q_R$  and  $\sigma$  can be directly attributed to the upper tropospheric warming that peaks around 200 hPa, implying that models with greater upper tropospheric warming (i.e., those models with large negative lapse rate feedback) have larger decreases in tropical high clouds. Furthermore, if a portion of the SW cloud feedback is due to changes in tropical high-cloud coverage, one would expect that portion of SW cloud feedback to be anticorrelated with the lapse

rate feedback: the larger the upper tropospheric warming, the larger the reduction in high cloud amount, and the smaller in magnitude the (negative) SW cloud feedback. This would allow one to define a combined lapse-rate SW cloud feedback that would have less intermodel spread than the two taken separately, in a similar way to the combined lapse rate–water vapor feedback. This is the subject of ongoing work that will be addressed in a subsequent paper. The remainder of the paper will focus on the implications of rising high-cloud tops for longwave cloud feedback.

[30] In Figure 6 we show tropical-mean *conv* and cloud fraction profiles for each of the 15 models used in this study. Assessing the degree to which the models exhibit a correspondence between their high-cloud fractions and the location of peak upper tropospheric *conv* is difficult because the model output available in the PCMDI archive is only the cloud fraction in the model vertical bins, with no information about optical depth or cloud top information similar to

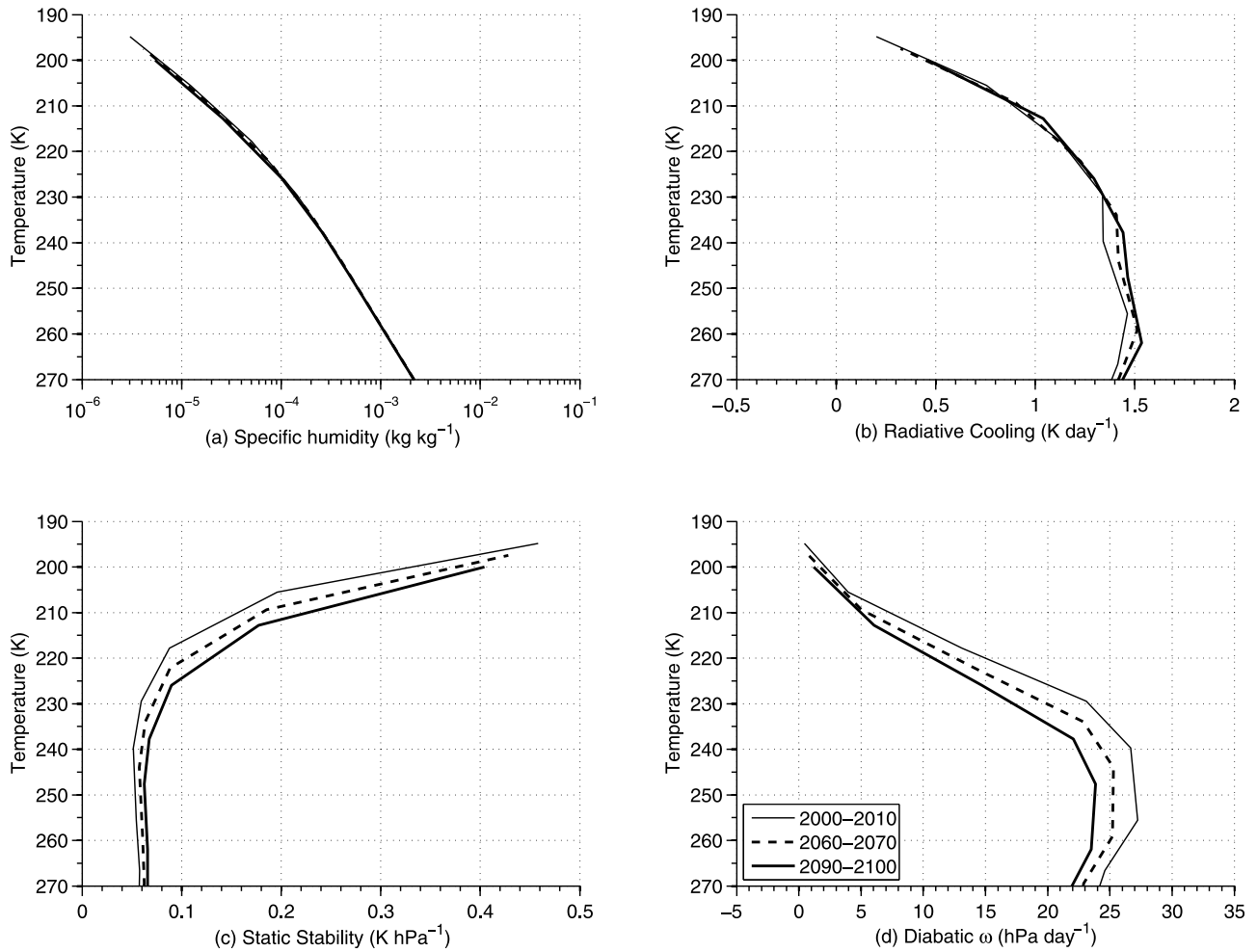


**Figure 4.** (a) Tropical-mean ensemble-mean specific humidity, (b) radiative cooling, (c) static stability, and (d) diabatic subsidence for 2000–2010 (thin solid), 2060–2070 (dashed), and 2090–2100 (thick solid) as a function of temperature. Ensemble-mean refers to the average over the 15 models that run the A2 scenario. Note that the specific humidity is plotted on a logarithmic scale and that temperature increases downward in each plot.

what a satellite sensor would retrieve in reality. It is also probable that each model defines cloud fraction differently. Thus, a lack of perfect correspondence between cloud fraction and upper tropospheric *conv* is not necessarily an indication that our diagnosis technique is flawed, nor is perfect correspondence a validation of our diagnosis technique. It is our hope that, in the future, modeling centers will archive more detailed cloud diagnostics that will be more useful than the cloud amounts shown here.

[31] Nonetheless, the models collectively produce a peak in high cloud amount that is consistent with the level diagnosed from the clear-sky energy and mass balance. Notable exceptions are the MIROC3.2(medres) model, where a large peak in cloud amount appears at the tropopause, most likely very thin tropopause cirrus that is disconnected from deep convection, and the MRI\_CGCM2.3.2a model, whose cloud fraction exhibits a very broad upper tropospheric peak that is rather different from its much sharper *conv* peak. In general, *conv* peaks are sharper and located at a slightly lower pressure than the cloud fraction peaks. It is reasonable

that a plot of cloud tops would exhibit a peak that is both sharper and located at lower pressures than the peak shown here for cloud amount. Thus, it is likely that a better correspondence exists between the level of abundant *conv* and the level of abundant high-cloud tops, the emission from which is more relevant for LW cloud feedback.

[32] Additionally, it is clear that all models produce cloud and *conv* profiles that remain nearly fixed in temperature. The models generally exhibit a slight decrease in upper tropospheric *conv* and cloud amount, though it appears as though the signal is larger in the *conv* profile.

[33] To assess the degree to which the upward migration of model clouds agrees with the upward migration of calculated *conv* in each model, we calculate the high cloud-weighted pressure and upper tropospheric clear-sky diabatic convergence-weighted pressure as

$$p_{\text{hield}} = \frac{\sum_{p \text{ at } T=270\text{K}}^{p \text{ at } \text{trop}} f * p}{\sum_{p \text{ at } T=270\text{K}}^{p \text{ at } \text{trop}} f} \quad (5)$$

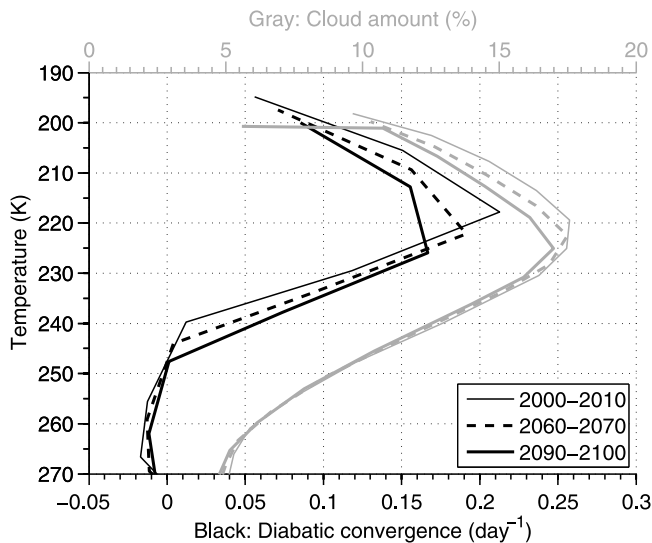


**Figure 5.** Tropical-mean ensemble-mean clear-sky diabatic convergence (black, bottom axis) and cloud amount (gray, top axis) for 2000–2010 (thin solid), 2060–2070 (dashed), and 2090–2100 (thick solid) as a function of temperature. Ensemble-mean refers to the average over the 15 models that run the A2 scenario. Note that temperature increases downward.

and

$$p_{conv} = \frac{\sum_p^{p \text{ at trop}} p \text{ at } T=270K \text{ conv} * p}{\sum_p^{p \text{ at trop}} p \text{ at } T=270K \text{ conv}}, \quad (6)$$

where  $f$  is the cloud fraction at each pressure. Scatterplots of decadal-mean tropical-mean  $p_{conv}$  and  $p_{hcloud}$  are shown for each model and for the ensemble mean in Figure 7. While the degree of correspondence between the location of abundant high cloud amount and upper tropospheric  $conv$  varies from model to model (Figure 6), the correspondence between the shift in  $p_{conv}$  and the shift in upper tropospheric  $p_{hcloud}$  as the climate warms is remarkably consistent from model to model, closely following a one-to-one relationship. In general, the decrease in  $p_{hcloud}$  is slightly larger than the decrease in  $conv$  weighted pressure. In other words, the clouds migrate slightly more than  $conv$  does.

[34] High cloud-weighted temperature ( $T_{hcloud}$ ) and upper tropospheric clear-sky diabatic convergence-weighted temperature ( $T_{conv}$ ) are calculated as in equations (5) and (6), but with  $T$  substituted for  $p$ . Scatterplots of decadal-mean tropical-mean upper tropospheric  $T_{conv}$  and  $T_{hcloud}$  are shown for each model and for the ensemble mean in Figure 8. Each number in the plot represents its respective decadal mean.

[35] As in Figure 8, the dashed line has slope one but nonzero  $y$  intercept. In  $T$  space, the shift in  $T_{conv}$  and  $T_{hcloud}$  is very small (on the order of a degree) indicating that both the high clouds and the upper tropospheric  $conv$  shift upward in altitude as the climate warms, but do so in such a way that they remain at approximately the same  $T$ . Because the  $conv$  profile migrates upward slightly less than the cloud profile, there is slightly greater warming of  $T_{conv}$  than of  $T_{hcloud}$ . This

is especially the case in the GFDL models, whose  $T_{hcloud}$ s remain remarkably constant in the face of relatively large increase of their  $T_{conv}$ s. Overall, the very slight shift toward warmer  $T_{hcloud}$  and  $T_{conv}$  is related to the increase in  $\sigma$  as the climate warms, as explained above. In summary, all models in the IPCC AR4 archive exhibit a clear shift in high cloud amount toward lower pressures that is remarkably well explained by the upper tropospheric  $conv$  inferred from radiative cooling. The shift occurs nearly isothermally, as expected from the FAT hypothesis.

[36] Figure 9, which plots the ensemble-mean  $T_{conv}$ ,  $T_{hcloud}$ , and the  $T$  at 200 hPa as a function of surface  $T$  over the course of the 21st century, concisely illustrates the main conclusions from the first part of this paper. Whereas the tropical upper troposphere warms 6 K, approximately twice as much as the mean tropical surface  $T$  (lapse rate feedback), the  $T_{hcloud}$  and  $T_{conv}$  warm only about 1 K. Tropical high clouds much more closely follow the isotherms rather than the isobars, as expected from the FAT hypothesis. This represents a strong positive feedback because the clouds are not warming in step with the surface or atmosphere; in other words, the planet cannot radiate away heat as easily as it could if the high clouds warmed along with the upper troposphere. In section 5 we make a quantitative estimate of the contribution of this nearly fixed  $T_{hcloud}$  to the total LW cloud feedback.

## 5. Estimating Actual and Hypothetical LW Cloud Feedbacks in the Models

[37] Though the tendency for clouds to shift upward as the climate warms has been noted in several previous studies [e.g., Hansen *et al.*, 1984; Wetherald and Manabe, 1988; Mitchell and Ingram, 1992; Senior and Mitchell, 1993], no study has explicitly shown to what extent this effect is giving rise to the positive LW cloud feedback. Here we make an estimate of the contribution to LW cloud feedback of the nearly constant  $T_{hcloud}$ . We first decompose the change in LW cloud forcing into its components, then calculate LW cloud feedback using the radiative kernel technique of Soden *et al.* [2008].

### 5.1. Contributors to the Change in LW Cloud Forcing

[38] The outgoing LW radiation ( $OLR$ ) can be written as the sum of contributions from the cloudy and clear regions, denoted by the subscripts  $cld$  and  $clr$ , respectively,

$$OLR = f_{tot}OLR_{cld} + (1 - f_{tot})OLR_{clr}, \quad (7)$$

where  $f_{tot}$  is the total cloud fraction output by the model. Note that this cloud fraction is the total (i.e., vertically integrated with overlap assumptions) cloud fraction to be distinguished from  $f$  which is the cloud fraction in each vertical bin. Because  $OLR$ ,  $OLR_{clr}$ , and  $f_{tot}$  are model diagnostics,  $OLR_{cld}$  is calculated using this equation. Note that  $OLR_{cld}$  is the LW radiation that is emerging from only the cloudy portion of the scene whereas  $OLR$  is the LW emerging from the entire scene including cloudy and clear subscenes. This allows us to define the  $LWCF$  as

$$LWCF = OLR_{clr} - OLR = f_{tot}(OLR_{clr} - OLR_{cld}). \quad (8)$$

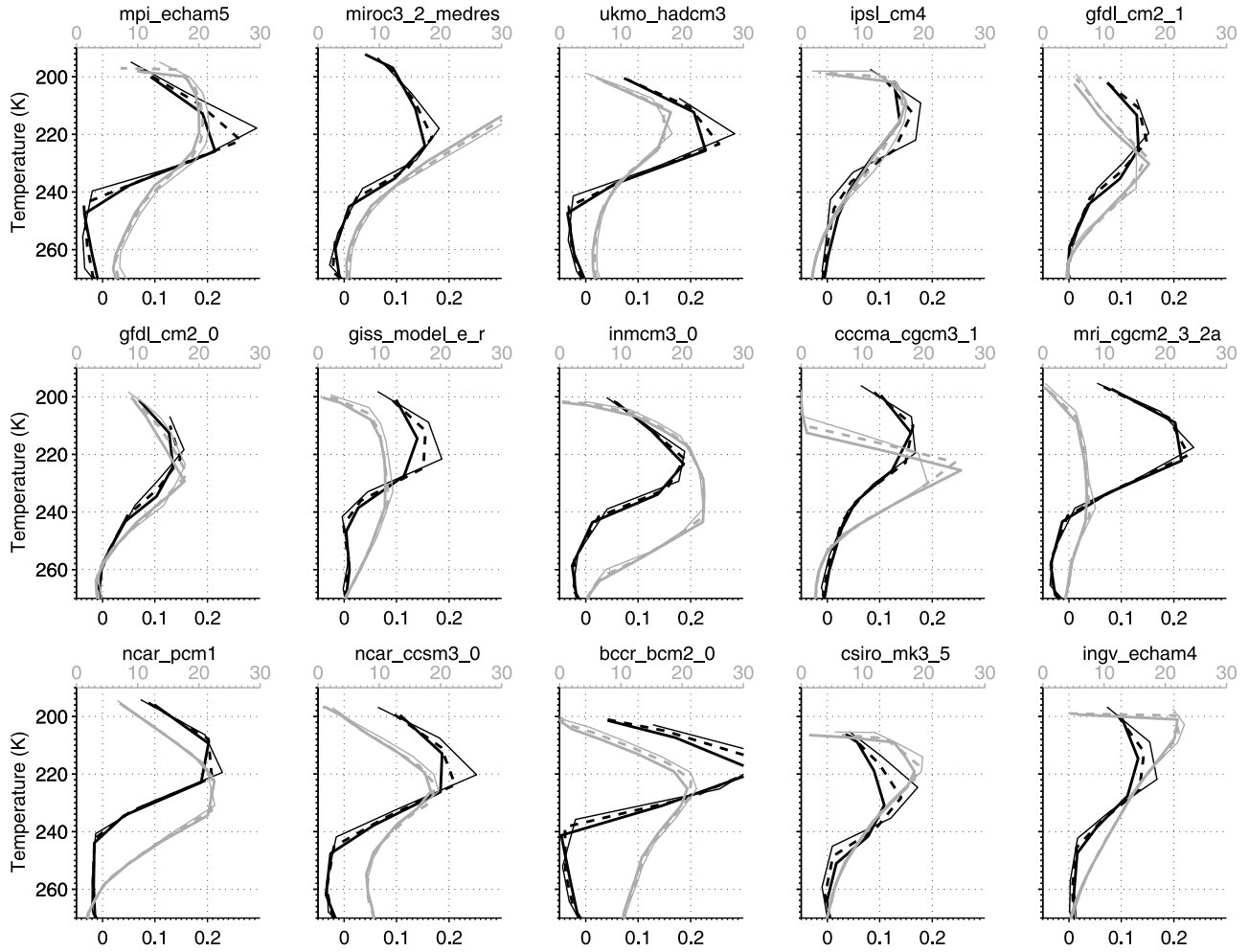


**Figure 6.** Tropical-mean clear-sky diabatic convergence (black, bottom axis) and cloud amount (gray, top axis) for 2000–2010 (thin solid), 2060–2070 (dashed), and 2090–2100 (thick solid) for the 15 IPCC AR4 models used in this study. The units for convergence are  $\text{day}^{-1}$  and for cloud amount are percent. Note that temperature increases downward in each plot.

[39] The change in  $LWCF$ , which we calculate as the difference between the 2090–2100 mean and the 2000–2010 mean, can be written as

$$\Delta LWCF = \Delta f_{tot}(OLR_{clr} - OLR_{cld}) + f_{tot}\Delta OLR_{clr} - f_{tot}\Delta OLR_{cld} + C. \quad (9)$$

The first term on the right hand side is the contribution from the change in cloud fraction assuming no change in clear minus cloudy  $OLR$ . This term is generally negative because cloud fraction decreases slightly. The second term is the change in clear-sky  $OLR$  assuming no change in cloud fraction. This term is generally positive in the extratropics and negative in the Tropics, as the atmosphere becomes more opaque to LW radiation. The third term is the change in cloudy-sky  $OLR$  assuming no change in cloud fraction. This term is strongly positive throughout most of the tropical oceans and negative elsewhere. That this term is so strongly positive throughout much of the Tropics implies that the cloudy-sky  $OLR$  decreases dramatically in many

regions as the climate warms. However, upon close inspection of the regions that show large values of  $\Delta OLR_{cld}$ , it is clear that the large changes are caused not by clouds cooling or warming but simply by increases or decreases in the relative amount of high versus low clouds. Because of this, we perform a slightly different decomposition below. The fourth term,  $C$ , is a covariance term, equal to  $\Delta f_{tot}\Delta OLR_{clr} - \Delta f_{tot}\Delta OLR_{cld}$ . It is negative on average throughout the Tropics.

[40] To better assess the relative roles of high and low clouds in affecting  $\Delta LWCF$ , we decompose  $OLR_{cld}$  into components due to high and low clouds in the Tropics,

$$f_{tot}OLR_{cld} = f_{hi}OLR_{hi} + f_{lo}OLR_{lo}, \quad (10)$$

where

$$f_{hi} + f_{lo} = f_{tot}. \quad (11)$$

Rather than attempting to calculate the high and low cloud fractions from the cloud amount profiles, we assume that the

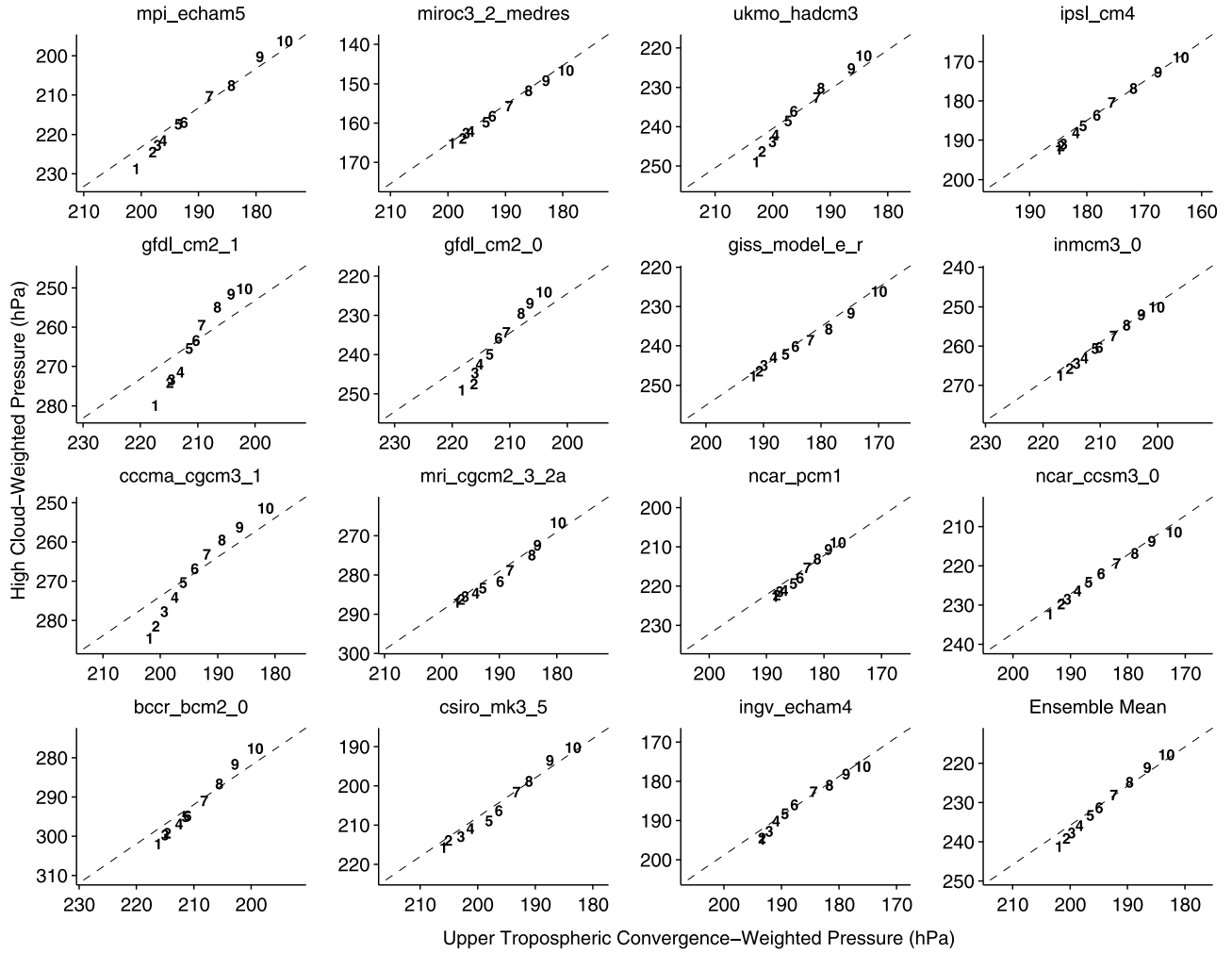


**Figure 7.** Scatterplots of tropical-mean decadal-mean upper tropospheric clear-sky diabatic convergence-weighted pressure and high cloud-weighted pressure for the 15 IPCC AR4 models used in this study as well as the ensemble mean. Each number identifies the respective decade within the 21st century. Note that pressure increases downward and to the left. The dashed line is a 1:1 line with a nonzero  $y$  intercept passing through the mean of both quantities.

high cloud-weighted temperature ( $T_{hi\text{cld}}$ ) is a reasonable estimate of the high-cloud emission  $T$  and that the cloud is a blackbody such that

$$OLR_{hi} = \sigma T_{hi\text{cld}}^4. \quad (12)$$

We also assume that the low cloud  $OLR$  is the same as the clear-sky  $OLR$ ,  $OLR_{lo} = OLR_{clr}$ . This allows us to calculate  $f_{hi}$  as

$$f_{hi} = f_{tot} \frac{OLR_{cld} - OLR_{lo}}{OLR_{hi} - OLR_{lo}} = f_{tot} \frac{OLR_{cld} - OLR_{clr}}{OLR_{hi} - OLR_{clr}}. \quad (13)$$

The decomposition of the change in LW cloud forcing is now

$$\Delta LWCF = \Delta f_{hi}(OLR_{clr} - OLR_{hi}) - f_{hi}\Delta OLR_{hi} + f_{hi}\Delta OLR_{clr} + C. \quad (14)$$

Thus, the change in  $LWCF$  is due to the change in  $f_{hi}$  assuming a constant difference between clear-sky  $OLR$  and

high-cloud  $OLR$ , the change in high-cloud  $OLR$  and clear-sky  $OLR$  assuming no change in  $f_{hi}$  and the covariance between changes in  $f_{hi}$ , high-cloud  $OLR$ , and clear-sky  $OLR$ .  $\Delta LWCF$  calculated here is exactly equal to that calculated directly.

[41] In Figure 10 we show the contribution of each of these components to the change in ensemble-mean  $LWCF$ . Note that the color scale varies among the plots to make the features more apparent. Henceforth, ensemble-mean refers to the average over the 12 models that run the A2 scenario and that archived enough information to compute cloud feedbacks. (Three of the models used previously do not output enough clear-sky diagnostics to compute cloud feedbacks.) Large regional changes in  $f_{hi}$  occur as the tropical circulation changes over the course of the century. Most notably,  $f_{hi}$  increases along the equatorial Pacific and Indian oceans are nearly compensated by  $f_{hi}$  decreases in the subtropics and over tropical landmasses (Figure 10a). Maps of both the mean and change in  $f_{hi}$  are very similar to maps of the mean and change in precipitation (not shown), lending

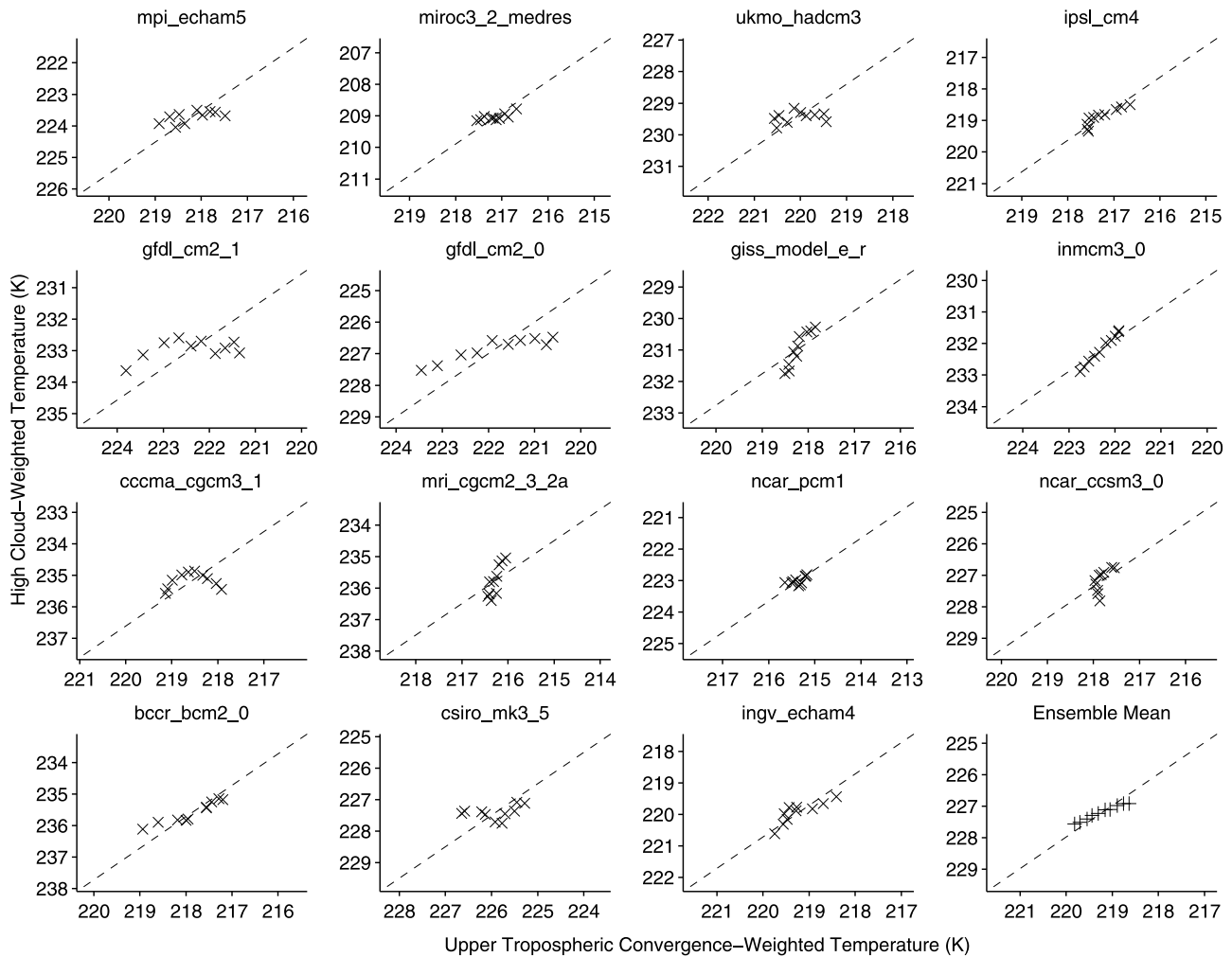


**Figure 8.** Scatterplots of tropical-mean decadal-mean upper tropospheric clear-sky diabatic convergence-weighted temperature and high cloud-weighted temperature for the 15 IPCC AR4 models used in this study as well as the ensemble mean. Each cross represents one decadal mean within the 21st century. Note that temperature increases downward and to the left. The dashed line is a 1:1 line with a nonzero  $y$  intercept passing through the mean of both quantities.

credence to our method of extracting the  $f_{hi}$  using equation (13). Overall, the redistribution of tropical high clouds tends to increase the  $LWCF$  in the Tropics (Figure 10a).

[42] In the Tropics, clear-sky  $OLR$  decreases between the beginning and end of the century as the atmosphere becomes more opaque (Figure 10b). This is especially true in convective regions that are moist in the free troposphere like over the western Pacific warm pool, resulting in a largely negative  $f_{hi}\Delta OLR_{clr}$  term. Because high-cloud temperatures do not stay perfectly constant with climate change as explained above, the  $-f_{hi}\Delta OLR_{hi}$  term is negative over most of the Tropics (Figure 10c). This is especially pronounced over the western Pacific warm pool and Indian Ocean. Taken together, the terms in Figures 10b and 10c represent a decrease in the difference between clear and cloudy  $OLR$  as the cloud tops warm slightly and the clear-sky  $OLR$  decreases slightly; thus they contribute to a decrease in  $LWCF$ .

[43] Both covariance terms (Figures 10d and 10e) are very small (note the color scale range) and systematically nega-

tive throughout the Tropics. These are due to the concurrent increase in  $f_{hi}$  in regions where both the high clouds are warming slightly and the clear-sky  $OLR$  is decreasing slightly.

[44]  $\Delta LWCF$  is negative throughout most of the Tropics, with two main regions of positive change, namely, the equatorial Pacific and off the east coast of Africa (Figure 10f). These two regions exhibit large increases in  $f_{hi}$  that outweigh the other terms contributing to  $\Delta LWCF$ . Over the maritime continent, the increase in high-cloud  $OLR$  and decrease in clear-sky  $OLR$  result in a decrease in  $LWCF$ . Over the tropical continents, the main cause of the decrease in  $LWCF$  is due to the decrease in  $f_{hi}$  as the climate warms.

## 5.2. From $\Delta LWCF$ to LW Cloud Feedback: Applying the Radiative Kernels

[45] The change in  $LWCF$  is not equal to the LW cloud feedback, though they are correlated [Soden *et al.*, 2004; Soden and Held, 2006]. Whereas  $\Delta LWCF$  is equal to the change in clear-sky minus all-sky  $OLR$ , the LW cloud

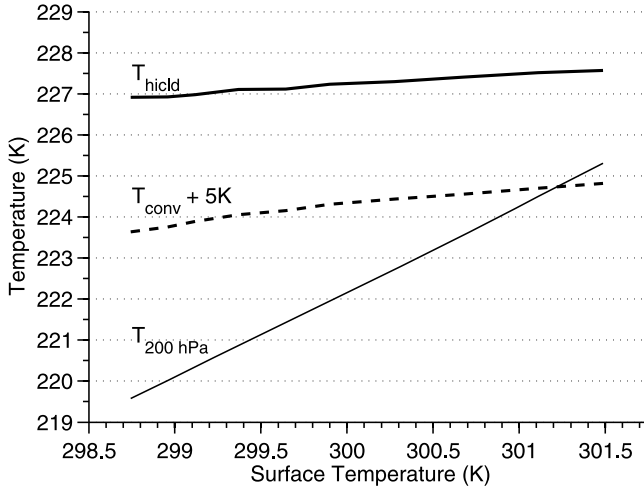


**Figure 9.** Tropical-mean ensemble-mean high cloud-weighted temperature (thick solid line), upper tropospheric clear-sky diabatic convergence-weighted temperature (dashed line), and 200 hPa temperature (thin solid line) plotted against tropical-mean ensemble-mean surface temperature for the 21st century. Ensemble-mean refers to the average over the 15 models that run the A2 scenario.

feedback is the change in  $OLR$  due to clouds alone. Thus, we calculate the LW cloud feedback by adjusting  $\Delta LWCF$  using the radiative kernel technique [Soden *et al.*, 2008]. Briefly, radiative kernels represent the LW or SW radiative response at the top of atmosphere to temperature, humidity, or surface albedo perturbations at each latitude, longitude, pressure (if applicable), and time. For each model we calculate the clear- and all-sky  $T$  and  $q$  feedbacks by convolving the appropriate radiative kernels with the change in  $T$  and  $q$  between the first and last decade of the 21st century. LW cloud feedback is estimated by adjusting the change in  $LWCF$  by the magnitude of cloud masking in the  $T$  and  $q$  feedbacks. The cloud masking is calculated by differencing the clear- and all-sky radiative responses and adding a term due to the cloud masking of the radiative forcing in the A2 scenario [Soden *et al.*, 2008, equation 25]. Assuming clouds mask the radiative forcing in the SRES A2 scenario (calculated by summing the A2 radiative forcing terms given in Tables 6.14 and 6.15 of the IPCC Third Assessment Report [Ramaswamy *et al.*, 2001]) by the same proportion as in the A1B scenario [Soden *et al.*, 2008], this term is  $1.03 \text{ W m}^{-2}$ .

### 5.3. Three Hypothetical LW Cloud Feedback Cases: FAT, FAP, and PHAT

[46] Here we compare three hypothetical scenarios to the actual  $\Delta LWCF$  to illustrate the contribution of nearly fixed high-cloud temperatures to the LW cloud feedback. We consider two cases that can be thought of as upper and lower bounds on  $\Delta LWCF$ , the fixed anvil temperature (FAT) and the fixed anvil pressure (FAP) cases, respectively. We also consider an intermediate case, the proportionately higher anvil temperature (PHAT) case, in which the change in  $T_{hicld}$  is set equal to the change in upper tropospheric  $T_{conv}$ . (Recall that the increase in  $T_{conv}$  is proportional to the increase of static stability that accompanies warming.) As

will be shown, PHAT does the best job of matching the LW cloud feedback in the models. Note that we use the term “anvil” very loosely to include all tropical high clouds, simply to maintain consistent terminology with Hartmann and Larson [2002].

[47] The change in  $LWCF$  assuming FAT is given by

$$\Delta LWCF_{FAT} = \Delta f_{hi}(OLR_{clr} - OLR_{hi}) + f_{hi}\Delta OLR_{clr} + C, \quad (15)$$

where the  $\Delta OLR_{hi}$  term in equation (14) is neglected because  $T_{hicld}$  is assumed fixed. The change in  $LWCF$  assuming FAP is given by

$$\Delta LWCF_{FAP} = \Delta f_{hi}(OLR_{clr} - OLR_{hi}) - f_{hi}\Delta OLR_{hi}^{FAP} + f_{hi}\Delta OLR_{clr} + C, \quad (16)$$

where  $\Delta OLR_{hi}^{FAP}$  is the change in high-cloud  $OLR$  assuming the clouds remain at the same pressure, the initial high cloud-weighted pressure, as the climate warms. The change in  $LWCF$  assuming PHAT is given by

$$\Delta LWCF_{PHAT} = \Delta f_{hi}(OLR_{clr} - OLR_{hi}) - f_{hi}\Delta OLR_{hi}^{PHAT} + f_{hi}\Delta OLR_{clr} + C, \quad (17)$$

where  $\Delta OLR_{hi}^{PHAT}$  is the change in high-cloud  $OLR$  assuming the change in  $T_{hicld}$  is equal to the change in tropical-mean  $T_{conv}$ . As we have seen, the change in  $T_{conv}$  is small but generally positive, so it represents a small but important correction to the FAT assumption. For all three cases, we compute  $\Delta LWCF$ , then apply the cloud mask corrections described above to calculate LW cloud feedback.

[48] In Figure 11 we plot maps of the ensemble mean LW cloud feedback estimated for each case, along with the difference between the actual LW cloud feedback and that computed for each case. Note that we use the term “actual” to refer to the model’s LW cloud feedback, not to the actual LW cloud feedback in nature. The decomposition of  $\Delta LWCF$  was only done for the Tropics, where it is easier to separate high and low clouds; thus the FAT, FAP, and PHAT assumptions differ only in the Tropics, due to the  $f_{hi}\Delta OLR_{hi}$  term. Strictly, the maps show the spatial structure of the LW cloud feedback, which is defined by globally integrating the local contributions.

[49] Unlike  $\Delta LWCF$ , the LW cloud feedback is positive throughout the Tropics, except in the FAP case where it is only positive over the equatorial Pacific and off the east coast of Africa where large increases in high clouds occur (Figure 11c). In the FAP feedback, the large increase in  $T_{hicld}$  results in a large negative contribution due to the change in  $OLR_{hi}$ . The FAP feedback is essentially that which would occur if the cloud profile did not shift upward as the climate warmed. Thus, the difference between the actual feedback and the FAP feedback shown in Figure 11d gives the contribution of changing cloud height to the LW cloud feedback. Here we find that the contribution to LW cloud feedback of the tendency for clouds *not* to warm as much as the upper troposphere is  $0.95 \text{ W m}^{-2} \text{ K}^{-1}$  in the tropical mean. Without this contribution, the tropical-mean LW cloud feedback would be negative, as shown in the FAP case.

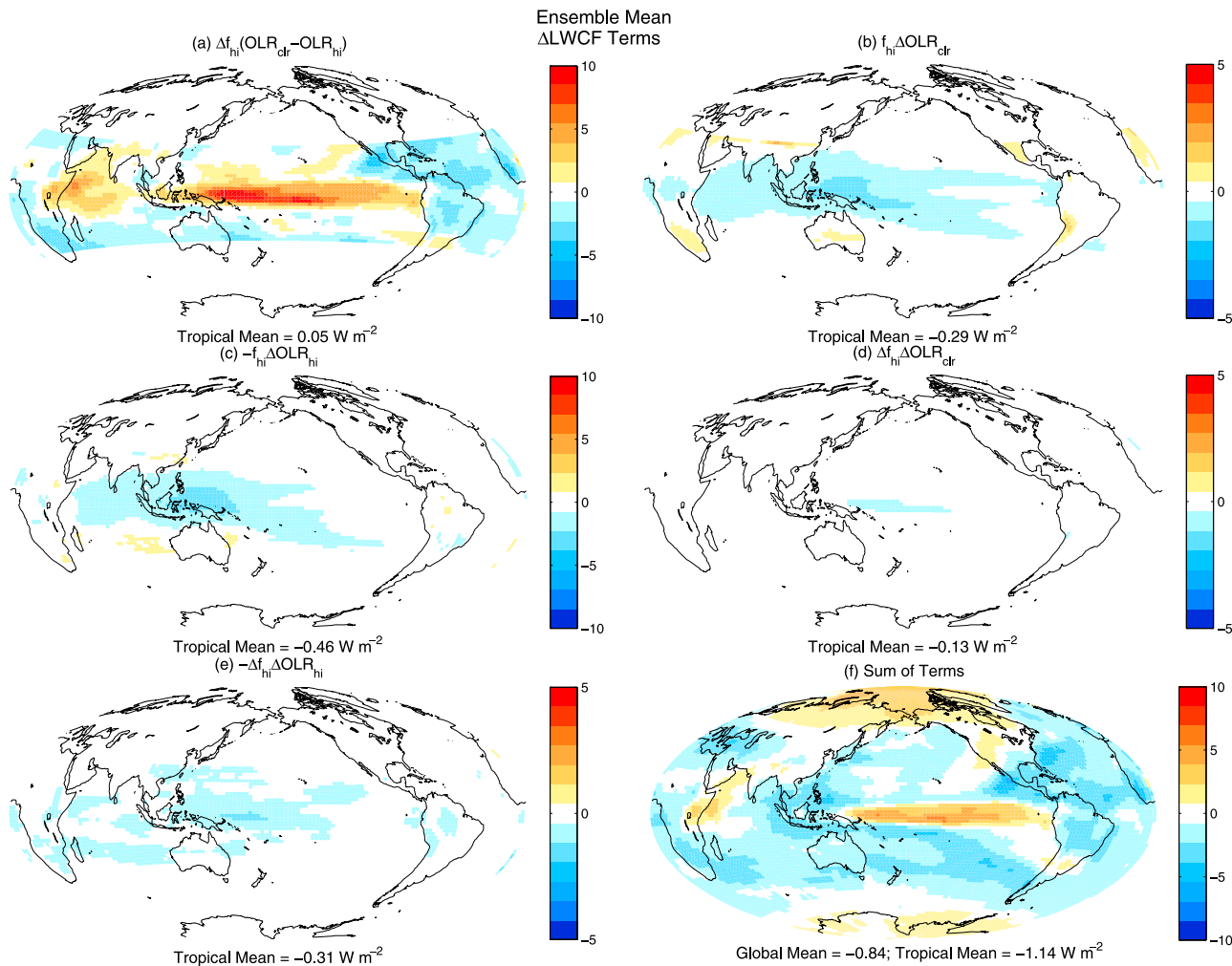


**Figure 10.** Terms contributing to the change in ensemble-mean  $LWCF$ : (a)  $\Delta f_{hi}(OLR_{clr} - OLR_{hi})$ , (b)  $f_{hi}\Delta OLR_{clr}$ , (c)  $-f_{hi}\Delta OLR_{hi}$ , (d)  $\Delta f_{hi}\Delta OLR_{clr}$ , (e)  $-\Delta f_{hi}\Delta OLR_{hi}$ , and (f) the sum of all terms, including the contribution from the extratropical terms that are not shown. Ensemble mean refers to the average over the 12 models that run the A2 scenario and that archived enough information to compute cloud feedbacks. Note that the color scale varies from plot to plot.

[50] The FAT feedback is slightly larger than the actual feedback because tropical high clouds do not stay at a fixed  $T$  as the climate warms (Figures 11a and 11b). Thus, a slight overestimate of the feedback occurs in all regions that have climatologically abundant high clouds. In the tropical mean, the FAT assumption overestimates the LW cloud feedback by  $0.27 \text{ W m}^{-2} \text{ K}^{-1}$ .

[51] Allowing tropical high clouds to warm along with the tropical-mean  $T_{conv}$  (i.e., PHAT) predicts a tropical-mean LW cloud feedback that is only slightly greater than the actual feedback by  $0.04 \text{ W m}^{-2} \text{ K}^{-1}$  (Figure 11f). Because we apply a spatially invariant tropical-mean warming to the high clouds in the PHAT assumption, there are some regions where we underestimate the feedback (i.e., over the continents and in the subtropics) and some regions where we overestimate the feedback (i.e., over the west Pacific warm pool and Indian Ocean). Where we overestimate the feedback, the high clouds warm more than does the tropical-mean upper tropospheric  $T_{conv}$ . Nevertheless, the feedback

calculated assuming PHAT agrees quite well with the actual LW cloud feedback, and properly accounts for the physics that govern the shift in the high-cloud profile.

[52] In Figure 12, we show bar plots of tropical- and global-mean LW cloud feedback along with the three cases FAP, PHAT, and FAT in each model and in the ensemble mean. Note that the feedback scenarios differ only in the Tropics, having the same LW feedback in the extratropics; the global-mean feedback is provided for completeness. Clearly, the feedback calculated assuming clouds remain at fixed pressure (FAP) greatly underestimates the actual LW cloud feedback. It is small in all models, with the spread being caused by differences in the other terms in the decomposition, most notably the change in  $f_{hi}$ . For nearly every model, the global-mean (tropical-mean) difference between FAP and actual feedback magnitude is about 0.5 (1.0)  $\text{W m}^{-2} \text{ K}^{-1}$ . This is entirely due to the fact that clouds do not stay at fixed pressure as the climate warms, but rather rise nearly isothermally.

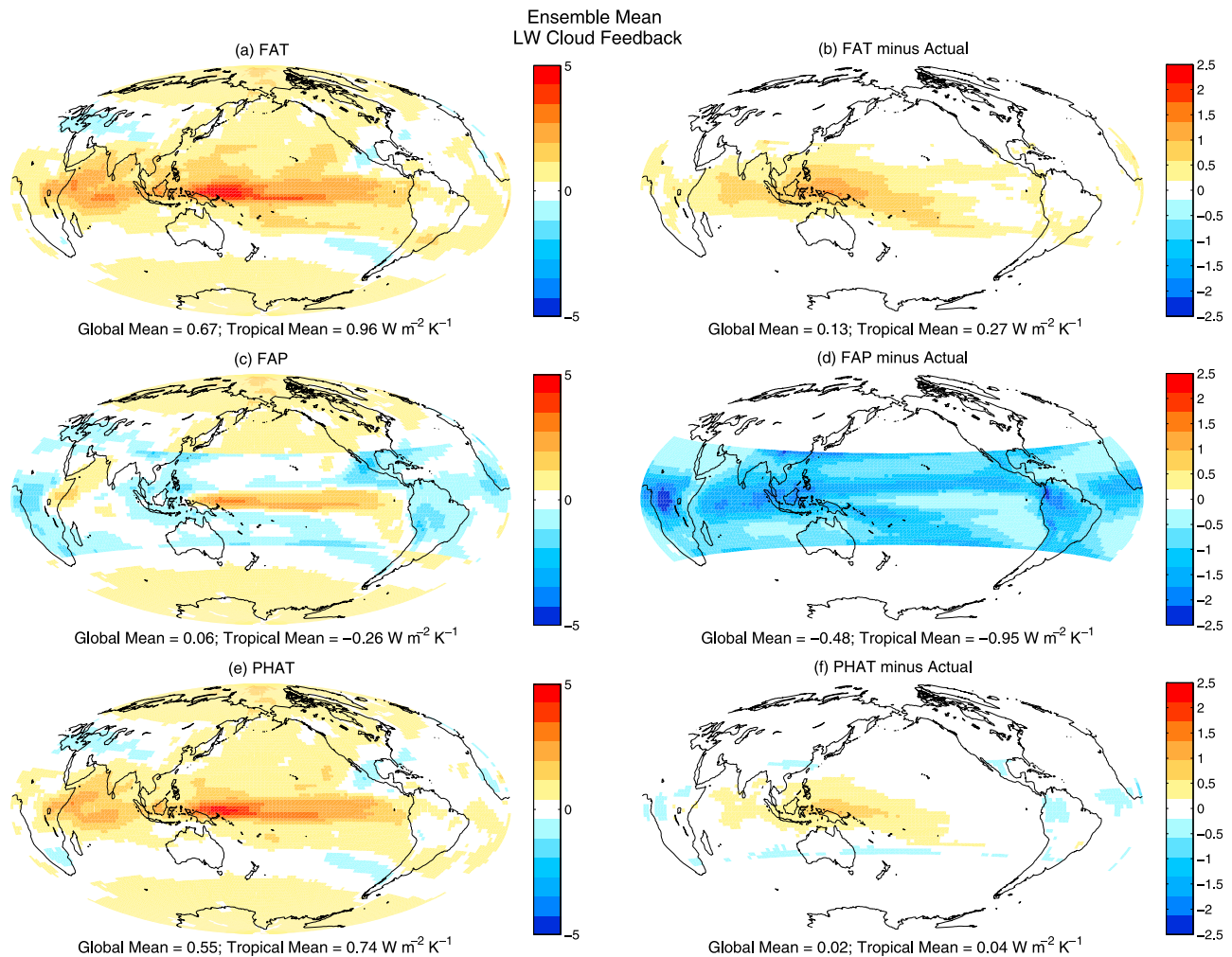


**Figure 11.** (a, c, and e) Ensemble-mean LW cloud feedback for three cases, FAT, FAP, and PHAT, as well as (b, d, and f) the difference between the actual LW cloud feedback and the three cases. Ensemble mean refers to the average over the 12 models that run the A2 scenario and that archived enough information to compute cloud feedbacks. Note the different color scales between Figures 11 (left) and 11 (right).

[53] On the other hand, the feedback calculated assuming  $T_{hield}$  does not change (i.e., FAT) slightly overestimates the LW cloud feedback in every model. The magnitude of overestimation varies from model to model depending on the degree to which the shift in cloud profile deviates from isothermal. In models with less pronounced upward enhancement of warming in the Tropics, the LW cloud feedback is closer to the value given by the FAT assumption because the reduction in pressure and corresponding increase in static stability at a fixed temperature is less, so that clouds warm less. FAT remains a considerably better approximation to the actual LW cloud feedback than FAP.

[54] The PHAT feedback very closely tracks the actual LW cloud feedback in all the models but can overestimate or underestimate the actual LW cloud feedback depending on how much each model's  $T_{conv}$  changes. In the ensemble mean, it is a slight overestimation, but is remarkably close to the actual value. The PHAT feedback is always positive, as there is a large contribution from the fact that the clouds do

not warm nearly as much as if they stayed at fixed pressure. PHAT is a slightly better predictor of the LW cloud feedback magnitude than FAT because it accounts for the change in  $\sigma$  that accompanies modeled climate change, thereby incorporating a slight increase of  $T_{hield}$ . Thus we have a physically consistent and robust predictor of each model's LW cloud feedback, and therefore high confidence that the systematically positive LW cloud feedback produced by the models is indeed correct.

## 6. Conclusions

[55] We have shown that tropical high clouds in models shift upward as the climate warms over the 21st century and that this upward shift is accompanied by a very modest increase in cloud top temperature. Because the clouds are not warming in step with the surface temperature, the warming Tropics become less efficient at radiating away

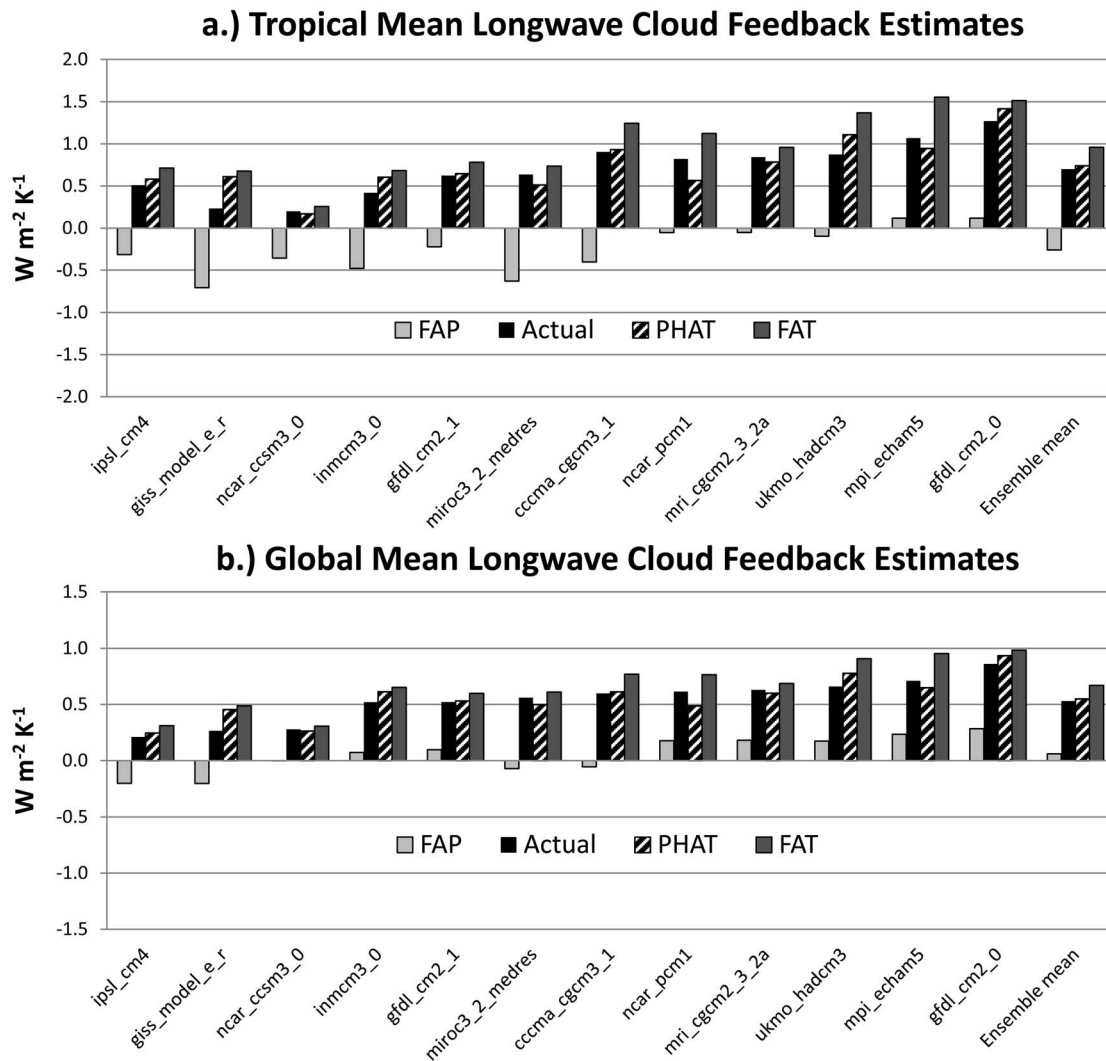


**Figure 12.** Estimates of (a) tropical-mean and (b) global-mean LW cloud feedback along with the three hypothetical cases FAP, FAT, and PHAT in each model and in the ensemble mean.

heat and thus the clouds are acting as a positive feedback on climate.

[56] The negligible temperature response of tropical high clouds to climate change can be understood through the principles of the fixed anvil temperature (FAT) hypothesis of *Hartmann and Larson* [2002]. The essential physics are simply that the troposphere can only be heated by convection where it is being cooled by radiation. Thus, clouds are only abundant in altitude ranges where the temperatures are high enough for appreciable water vapor to radiatively cool to space. If the entire troposphere warms, the tropical-mean cloud tops will be located at a higher altitude that is now warm enough that water vapor near saturation has substantial LW emissivity.

[57] Assuming a mass conserving circulation connects the convective and nonconvective regions of the Tropics, the altitude of convective detrainment and abundant high cloud amount must be colocated with the altitude of strong radiatively driven convergence, *conv*. One can calculate the *conv* profile in a relatively straightforward manner by computing the vertical gradient of the diabatic subsidence,

$\omega$ , required to balance radiative cooling,  $Q_R$ . Because of the rapid falloff of  $Q_R$  and rapid increase of static stability,  $\sigma$ , with decreasing pressure, diabatic  $\omega$  decreases rapidly with decreasing pressure in the upper troposphere, creating a region of enhanced *conv*. We have shown good qualitative agreement between this level of enhanced upper tropospheric *conv* and the high cloud amount in each model.

[58] As the climate warms over the course of the 21st century,  $p_{conv}$  and  $p_{hield}$  decrease in a nearly one-to-one fashion, and do so in such a way as to remain at approximately the same  $T$ . Because the vertical structure of changes to the  $Q_R$  profile differs from that of the  $\sigma$  profile, the diabatic  $\omega$  decreases below and increases above the level of peak *conv*, causing a decrease in *conv* that is mimicked by slight decreases the upper tropospheric cloud fraction. Both the clouds and *conv* tend to warm slightly over the course of the century, and this is due to an increase in  $\sigma$  that prevents the clouds from rising isothermally.

[59] To assess the contribution of nearly constant cloud top temperatures to the LW cloud feedback, we first decomposed the change in *LWCF* into components. This

allowed us to create three cases, one in which  $T_{high}$  (and therefore high cloud-*OLR*) does not change (FAT), one in which  $T_{high}$  increases as much as does the temperature at a fixed pressure level (FAP), and one in which  $T_{high}$  increases along with the tropical-mean upper tropospheric  $T_{conv}$  (PHAT).

[60] Assuming that clouds do not rise as the climate warms (i.e., FAP) results in a near-zero LW cloud feedback in every model. The global-mean (tropical-mean) LW cloud feedback is systematically about 0.5 (1.0)  $\text{W m}^{-2} \text{K}^{-1}$  larger than that calculated assuming FAP, and this is entirely because high clouds rise in such a way as to warm only slightly in every model. The LW cloud feedback calculated assuming FAT slightly overestimates the actual LW cloud feedback because the  $T_{high}$  does increase slightly over the course of the century. That calculated assuming PHAT is very close to the actual LW cloud feedback in all models and represents an improved estimate over FAT because it allows for the slight increase in  $T_{high}$  due to the increase in static stability. Thus, we show that the robust positive LW cloud feedback can be well explained by the fundamental physics of FAT, with a slight modification (PHAT) to take into account the modeled static stability changes. Tropical high clouds are fundamentally constrained to emit at approximately the same temperature as the climate warms, and we have shown here that this results in a LW cloud feedback that is robustly positive in climate models.

[61] **Acknowledgments.** This research was supported by NASA Earth and Space Science Fellowship NNX06AF69H and NASA Grant NNX09AH73G. We acknowledge the international modeling groups for providing their data for analysis, the Program for Climate Model Diagnosis and Intercomparison (PCMDI) for collecting and archiving the model data, and B. J. Soden for providing the radiative kernels. We thank Chris Bretherton, Rob Wood, Andrew Dessler, and two anonymous reviewers for useful suggestions for improvement, as well as Marc Michelsen for computer support.

## References

- Ackerman, T. P., K. N. Liou, F. P. J. Valero, and L. Pfister (1988), Heating rates in tropical anvils, *J. Atmos. Sci.*, *45*, 1606–1623.
- Bergman, J. W., and H. H. Hendon (1998), Calculating monthly radiative fluxes and heating rates from monthly cloud observations, *J. Atmos. Sci.*, *55*, 3471–3491.
- Bony, S., and J. L. Dufresne (2005), Marine boundary layer clouds at the heart of tropical cloud feedback uncertainties in climate models, *Geophys. Res. Lett.*, *32*, L20806, doi:10.1029/2005GL023851.
- Bony, S., et al. (2006), How well do we understand and evaluate climate change feedback processes?, *J. Clim.*, *19*, 3445–3482.
- Cess, R. D., et al. (1990), Intercomparison and interpretation of cloud-climate feedback processes in nineteen atmospheric general circulation models., *J. Geophys. Res.*, *95*, 16,601–16,615.
- Chae, J. H., and S. C. Sherwood (2010), Insights into cloud-top height and dynamics from the seasonal cycle of cloud-top heights observed by MISR in the West Pacific region, *J. Atmos. Sci.*, *67*, 248–261.
- Colman, R. (2003), A comparison of climate feedbacks in general circulation models, *Clim. Dyn.*, *20*, 865–873.
- Eitzen, Z. A., K. M. Xu, and T. Wong (2009), Cloud and radiative characteristics of tropical deep convective systems in extended cloud objects from CERES observations, *J. Clim.*, *22*, 5983–6000.
- Folkins, I., and R. Martin (2005), The vertical structure of tropical convection and its impact on the budgets of water vapor and ozone, *J. Atmos. Sci.*, *62*, 1560–1573.
- Fu, Q., and K. N. Liou (1992), On the correlated k-distribution method for radiative transfer in nonhomogeneous atmospheres, *J. Atmos. Sci.*, *49*, 2139–2156.
- Gastineau, G., L. Li, and H. L. Treut (2009), The Hadley and Walker circulation changes in global warming conditions described by idealized atmospheric simulations, *J. Clim.*, *22*, 3993–4013.
- Hansen, J., A. Lacis, D. Rind, G. Russell, P. Stone, I. Fung, R. Ruedy, and J. Lerner (1984), Climate sensitivity: Analysis of feedback mechanisms, in *Climate Processes and Climate Sensitivity*, *Geophys. Monogr. Ser.*, vol. 29, edited by J. E. Hansen and T. Takahashi, pp. 130–163, AGU, Washington, D. C.
- Hartmann, D. L., and K. Larson (2002), An important constraint on tropical cloud-climate feedback, *Geophys. Res. Lett.*, *29*(20), 1951, doi:10.1029/2002GL015835.
- Hartmann, D. L., J. R. Holton, and Q. Fu (2001), The heat balance of the tropical tropopause, cirrus, and stratospheric dehydration, *Geophys. Res. Lett.*, *28*, 1969–1972, doi:10.1029/2000GL012833.
- Held, I. M., and B. J. Soden (2006), Robust responses of the hydrological cycle to global warming, *J. Clim.*, *19*, 5686–5699.
- Knutson, T. R., and S. Manabe (1995), Time-mean response over the tropical Pacific to increased  $\text{CO}_2$  in a coupled ocean-atmosphere model, *J. Clim.*, *8*, 2181–2199.
- Kuang, Z., and D. L. Hartmann (2007), Testing the fixed anvil temperature hypothesis in a cloud-resolving model, *J. Clim.*, *20*, 2051–2057.
- Kubar, T. L., D. L. Hartmann, and R. Wood (2007), Radiative and convective driving of tropical high clouds, *J. Clim.*, *20*, 5510–5526.
- L'Ecuyer, T. S., and G. McGarragh (2010), A 10-year climatology of tropical radiative heating and its vertical structure from TRMM observations, *J. Clim.*, *23*, 519–541.
- Minschwaner, K., and A. E. Dessler (2004), Water vapor feedback in the tropical upper troposphere: Model results and observations, *J. Clim.*, *17*, 1272–1282.
- Mitchell, J. F. B., and W. J. Ingram (1992), Carbon dioxide and climate: Mechanisms of changes in cloud, *J. Clim.*, *5*, 5–21.
- Ramaswamy, V., et al. (2001), Radiative forcing of climate change, in *Climate Change 2001: The Scientific Basis*, edited by J. T. Houghton et al., pp. 350–416, Cambridge Univ. Press, Cambridge, U. K.
- Senior, C. A., and J. F. B. Mitchell (1993), Carbon dioxide and climate: The impact of cloud parameterization, *J. Clim.*, *6*, 393–418.
- Soden, B. J., and I. M. Held (2006), An assessment of climate feedbacks in coupled ocean-atmosphere models, *J. Clim.*, *19*, 3354–3360.
- Soden, B. J., A. J. Broccoli, and R. S. Hemler (2004), On the use of cloud forcing to estimate cloud feedback, *J. Clim.*, *17*, 3661–3665.
- Soden, B. J., I. M. Held, R. Colman, K. M. Shell, J. T. Kiehl, and C. A. Shields (2008), Quantifying climate feedbacks using radiative kernels, *J. Clim.*, *21*, 3504–3520.
- Sohn, B.-J. (1999), Cloud-induced infrared radiative heating and its implications for the large-scale tropical circulation, *J. Atmos. Sci.*, *56*, 2657–2672.
- Stephens, G. L., A. Slingo, M. J. Webb, P. J. Minnett, P. H. Daum, L. Kleinman, I. Wittmeyer, and D. A. Randall (1994), Observations of the Earth's Radiation Budget in relation to atmospheric hydrology 4: Atmospheric column radiative cooling over the world's oceans, *J. Geophys. Res.*, *99*, 18,585–18,604.
- Tompkins, A. M., and G. C. Craig (1999), Sensitivity of tropical convection to sea surface temperature in the absence of large-scale flow, *J. Clim.*, *12*, 462–476.
- Trenberth, K. E., and J. T. Fasullo (2009), Global warming due to increasing absorbed solar radiation, *Geophys. Res. Lett.*, *36*, L07706, doi:10.1029/2009GL037527.
- Vecchi, G. A., and B. J. Soden (2007), Global warming and the weakening of the tropical circulation, *J. Clim.*, *20*, 4316–4340.
- Webb, M. J., et al. (2006), On the contribution of local feedback mechanisms to the range of climate sensitivity in two GCM ensembles, *Clim. Dyn.*, *27*, 17–38.
- Wetherald, R., and S. Manabe (1988), Cloud feedback processes in a general circulation model, *J. Atmos. Sci.*, *45*, 1397–1415.
- Xu, K. M., and K. A. Emanuel (1989), Is the tropical atmosphere conditionally unstable?, *Mon. Weather Rev.*, *117*, 1471–1479.
- Xu, K. M., T. Wong, B. A. Wielicki, L. Parker, and Z. A. Eitzen (2005), Statistical analyses of satellite cloud object data from CERES. Part I: Methodology and preliminary results of the 1998 El Niño/2000 La Niña, *J. Clim.*, *18*, 2497–2514.
- Xu, K. M., T. Wong, B. A. Wielicki, L. Parker, B. Lin, Z. A. Eitzen, and M. Branson (2007), Statistical analyses of satellite cloud object data from CERES. Part II: Tropical convective cloud objects during 1998 El Niño and evidence for supporting the fixed anvil temperature hypothesis, *J. Clim.*, *20*, 819–842.

D. L. Hartmann and M. D. Zelinka, Department of Atmospheric Sciences, University of Washington, Box 351640, Seattle, WA 98195, USA. (mzelinka@atmos.washington.edu)